Comparison of the PPMXL and UCAC5 Catalogs with the *Gaia* DR2

Y.-Y. Shi, Z. Zhu ⓘ, N. Liu, J.-C. Liu ⓘ, C.-Y. Ding, and Y.-T. Cheng
School of Astronomy and Space Science, Key Laboratory of Modern Astronomy and Astrophysics (Ministry of Education), Nanjing University, 163 Xianlin Avenue, 210023 Nanjing, People's Republic of China; zhuzi@nju.edu.cn

Abstract

Astrometric ground-based catalogs usually suffer from varied systematic errors. These systematic errors were hard to detect because there was no independent reference catalog complete to very faint limiting magnitudes (∼20 mag). This situation has changed since the second data release of the *Gaia* mission (*Gaia* DR2). We aim to investigate positions and the proper-motion (PM) system of two ground-based catalogs, the UCAC5 and PPMXL, referring to the *Gaia* DR2. The individual position in the *Gaia* DR2 is transferred by its PM to the epoch of other catalogs for comparison. Systematic errors that depend on the magnitude, color, and sky regions in the UCAC5 and PPMXL could be clearly seen. A different behavior between the northern and southern sky is found in the PPMXL, which is possibly inherited from the imperfect calibration of the PM system. Besides, we perform a quantitative analysis of global differences for positions and PMs by the vector spherical harmonics method in terms of 3 rotation angles, 3 glide parameters, and 10 quadrupole parameters. We find a large glide component of ∼8 mas along Z-axis and a rotation angle of ∼5 mas about Z-axis for positional offsets between the PPMXL and *Gaia* DR2. These terms are found to be insignificant between the UCAC5 and *Gaia* DR2. We show that the position and PM system of the UCAC5, a new reduction of ground-based observations in the frame of the *Gaia* reference system, has been largely improved. This indicates that systematic errors in positions and PMs obtained from ground-based observations are mostly impacted by a relatively poor reference catalog. But these observations can be reconstructed in the frame of a space-based reference catalog. In this sense, our results justify the tradition of space-calibrated ground-based astrometric catalogs.

Key words: astrometry – catalogs – proper motions – reference systems

1. Introduction

The all-sky ground-based astrometric surveys started from the end of the 19th century, dating back to the initiation of the Astrographic Catalog (AC) project in 1887. One of the motivations of such projects is to construct fundamental catalogs that represent the best possible approximations to the inertial reference system. One example is the Fifth Fundamental Catalog (FK5), which is constructed by transit circle observations independently and provided a basic stellar reference frame as adopted by the International Astronomical Union (Fricke et al. 1988). Later in 1997, the FK5 system was replaced by the *Hipparcos* Catalog (ESA 1997) as the primary optical realization of the International Celestial Reference System (ICRS; Ma et al. 1998). The aim of the astrometric community has been changed to extend the *Hipparcos* system to higher star densities and fainter limiting magnitudes since then. The first and most important catalog is the Tycho-2 (Høg et al. 2000), based on the old-epoch observations from the AC project and observations from the Tycho experiment in the ESA-*Hipparcos* mission. The Tycho-2 catalog usually serves as the representative of the ICRS system, on which many catalogs complete down to fainter limiting magnitudes were built. In addition, there are two widely used series of catalogs; they are the extensions of *Hipparcos* system: series of the United States Naval Observatory CCD Astrograph Catalog (UCAC series) (e.g., Zacharias et al. 2013), and the PPM series consisted of PPM (Röser & Bastian 1993), PPMX (Röser et al. 2008), and PPMXL (Roeser et al. 2010).

On the contrary, space observations have been developed in just a few decades. The *Hipparcos* mission (ESA 1997) is the very first space mission measuring the absolute parallax with unprecedented accuracy (milliarcsecond) for over 100,000 objects. The *Hipparcos* catalog was adopted to be the primary realization of the ICRS at the optical wavelength (Perryman et al. 1997). The success of the *Hipparcos* mission shows the surprising advantages of the space observation technique. Then comes ESA astrometric successor mission, *Gaia*. The *Gaia* Data Release 1 (*Gaia* DR1; Gaia Collaboration et al. 2016a, 2016b), published in 2016, provided astrometry and photometry information for over 1 billion sources, but only 2 million sources in the TGAS catalog have proper motions. In 2018, the *Gaia* Data Release 2 (*Gaia* DR2; Gaia Collaboration et al. 2018) was published. Astrometric and astrophysical data for more than 1.69 billion sources are now available.

It is well known that the ground-based astrometric observations suffer from magnitude-, color-, and sky-location-dependent systematic errors, and the disturbing effects of the Earth's atmosphere (Roeser et al. 2010). These systematic errors could be studied with the reference of the space surveys (catalogs). For instance, Zhu (2000) and Mignard & Frœschlé (2000) studied the FK5 catalog with the *Hipparcos* catalog and found significant zonal errors in the position and proper motion of the FK5 system. Now the astrometric catalogs usually have faint limiting magnitudes of about ∼20 mag, for example, PPMXL, where the *Hipparcos* catalog cannot be used as the reference. Instead, the analyses of the systematics in these catalogs are performed by intercomparisons. Liu et al. (2011) analyzed the systematic differences between the PPMX and UCAC3 catalogs and found systematic errors in the northern hemisphere of the UCAC3. Series of intercomparisons between the UCAC4, PPMXL, and XPM were also carried out (Vityazev & Tsvetkov 2014, 2015, 2016; Vityazev et al. 2017). These comparisons, however, were performed without an independent

1

external check. This situation is changed since the publication of the *Gaia* DR2. As a new optical realization of the ICRS, the *Gaia* DR2 enables us to analyze the systematic differences of previous large optical catalogs thanks to its high internal consistency of stellar positions, proper motions, and parallax system. Since the release of *Gaia* DR1, there have been catalogs reconstructed by combining the ground-based observations and the *Gaia* observations, which help improve the earlier astrometric catalog data. In this paper, we aim to address the systematic errors in the large ground-based astrometric catalogs and illustrate the improvements of old observations calibrated by the *Gaia* observations. The PPMXL is chosen as the representative of the ground-based compiled catalog while UCAC5 is used to represent the combination of the ground- and space-based catalogs.

In Section 2, we introduce the cross-match process of the UCAC5 and PPMXL catalogs with the *Gaia* DR2 and calculate the individual offsets in positions and PMs. Then we investigate the position and PM offsets as functions of the magnitude and color system (Section 3) and on the global and regional scales (Section 4). In Section 5, additional comparisons were made. Finally, some concluding remarks are presented in Section 6.

2. Catalogs and Cross-match

The *Gaia* DR2 catalog provides the full astrometric parameters (positions, proper motions, and parallaxes) for about 1.3 billion sources with a limiting magnitude of $G = 21$. The median uncertainty is about 0.04 mas for parallaxes and positions at J2015.5 and 0.05 mas yr^{-1} for PMs for bright sources ($G < 15$ mag; Lindegren et al. 2018). The B$-$R (BP$-$RP) color information for approximately 1.4 billion sources is also available (Riello et al. 2018). The *Gaia* DR2 has built a rotation-free celestial reference frame (*Gaia*-CRF2) in optical wavelengths. It is consistent with the ICRS and is nonrotating with respect to the quasars within 0.15 mas yr^{-1} (Lindegren et al. 2018).

The UCAC5 is the latest astrometric reduction of the UCAC all-sky observations (Zacharias et al. 2017). In its previous version UCAC4, the reference star catalog for the wide-field CCD observations is the Tycho-2 catalog. However, Tycho-2 was proved to have sky-correlated systematic errors as large as a few mas yr^{-1} as seen from the TGAS catalog (Lindegren et al. 2016). To improve the astrometric precision, the UCAC5 used the latest TGAS as the reference. Finally, over 107 million stars were obtained and the typical accuracies of proper motions are 1–2 mas yr^{-1} ($R \approx 11$–15 mag), and $\sim$5 mas yr^{-1} at 16 mag. Formal positional errors are about 8 mas ($G = 11$ mag), 20 mas ($G = 14$ mag), and 60 mas ($G = 16$ mag). The systematic errors as a function of magnitude in the UCAC5, as pointed out in Zacharias et al. (2017), comes from the poor charge transfer efficiency of the CCDs. This remaining systematic error, however, is expected not to exceed 10 mas in positions, which corresponds to systematic errors in PMs up to 0.7 mas yr^{-1}.

The PPMXL is a catalog containing positions, proper motions and optical photometry of 900 million stars and galaxies with a complete sky coverage down to 20th magnitude (Roeser et al. 2010). It originated from the United States Naval Observatory B1.0 Catalog (USNO-B1.0) (Monet et al. 2003) and Two Micron All-Sky Survey (2MASS; Skrutskie et al. 2006). The data of USNO-B1.0 were obtained from scans of

7435 Schmidt plates (Monet et al. 2003). The typical individual mean errors of the proper motions range from 4 mas yr^{-1} to larger than 10 mas yr^{-1}, depending on the observational time length. The mean errors of the positions at epoch J2000.0 are estimated to be 80–120 mas for 410 million sources whose positions can be obtained from the 2MASS catalog, while for the others are about 150–300 mas.

Our cross-match process is based on the cross-match results from previous works instead of performing a direct cross-match. The UCAC5 provides the source_id of the corresponding entry in the *Gaia* DR1, while the source_id identifier systems in the *Gaia* DR1 and DR2 are totally different and independent. The link between the *Gaia* DR1 and DR2 entries could be found in the *Gaia* data archive.[1] So we cross-matched the entries in the UCAC5 and the *Gaia* DR2 catalogs via the *Gaia* DR1 identifier. A cross-match list between the *Gaia* DR2 and PPMXL can be found in Marrese et al. (2019).[2] In addition, only sources that have five astrometric parameters and the one matched source in the UCAC5/PPMXL catalog in the *Gaia* DR2 were kept. Finally, we obtained 106,617,488 common objects in the *Gaia* DR2 and UCAC5 catalog, and 631,626,536 common objects in the *Gaia* DR2 and PPMXL catalog.

The individual position in the *Gaia* DR2 is transferred to the epoch of other catalogs for comparison by the proper motion of *Gaia* DR2. The position offsets of the UCAC5 and PPMXL referring to the *Gaia* DR2 are calculated as follows

$$\Delta\alpha^* = \{\alpha_i - [\alpha_{\text{GDR2}} - (T_{\text{GDR2}} - T_i) \times \mu_{\alpha,\text{GDR2}}]\}$$
$$\times \cos\delta_{\text{GDR2}},$$
$$\Delta\delta = \delta_i - [\delta_{\text{GDR2}} - (T_{\text{GDR2}} - T_i) \times \mu_{\delta,\text{GDR2}}], \quad (1)$$

where the subscript "GDR2" represents the *Gaia* DR2, the subscript "i" for the UCAC5 or PPMXL, and T_i for the epoch of individual stars. The proper-motion differences can be written as

$$\Delta\mu_\alpha^* = (\mu_{\alpha,i} - \mu_{\alpha,\text{GDR2}}) \times \cos\delta_{\text{GDR2}},$$
$$\Delta\mu_\delta = \mu_{\delta,i} - \mu_{\delta,\text{GDR2}}. \quad (2)$$

3. Magnitude- and Color-dependent Systematic Errors

In this section, we analyze the magnitude- and color-dependent systematic errors of stellar positions and PMs in the UCAC5 and PPMXL catalogs. First, we divided the sources into six decl. belts by an interval of 30° to analyze the decl.-dependent differences. In each decl. belt, we binned the common stars by the G magnitude or B$-$R color because of the enormous number of sources. We chose different bin sizes for the UCAC5 and PPMXL considering that the number of common sources between the PPMXL and *Gaia* DR2 is much larger than that for the UCAC5 and *Gaia* DR2. The bin size is 50,000 for the UCAC5 and 200,000 for the PPMXL. In each bin, we calculated the root mean square (rms) of position and proper-motion differences of all entries and removed entries whose position or PM offset is 3 times greater than the corresponding rms. Then we computed the mean difference of stellar coordinates and PMs in each bin.

---

[1] Please find the list at http://gea.esac.esa.int/archive/.
[2] The list can be found at http://gea.esac.esa.int/archive/.
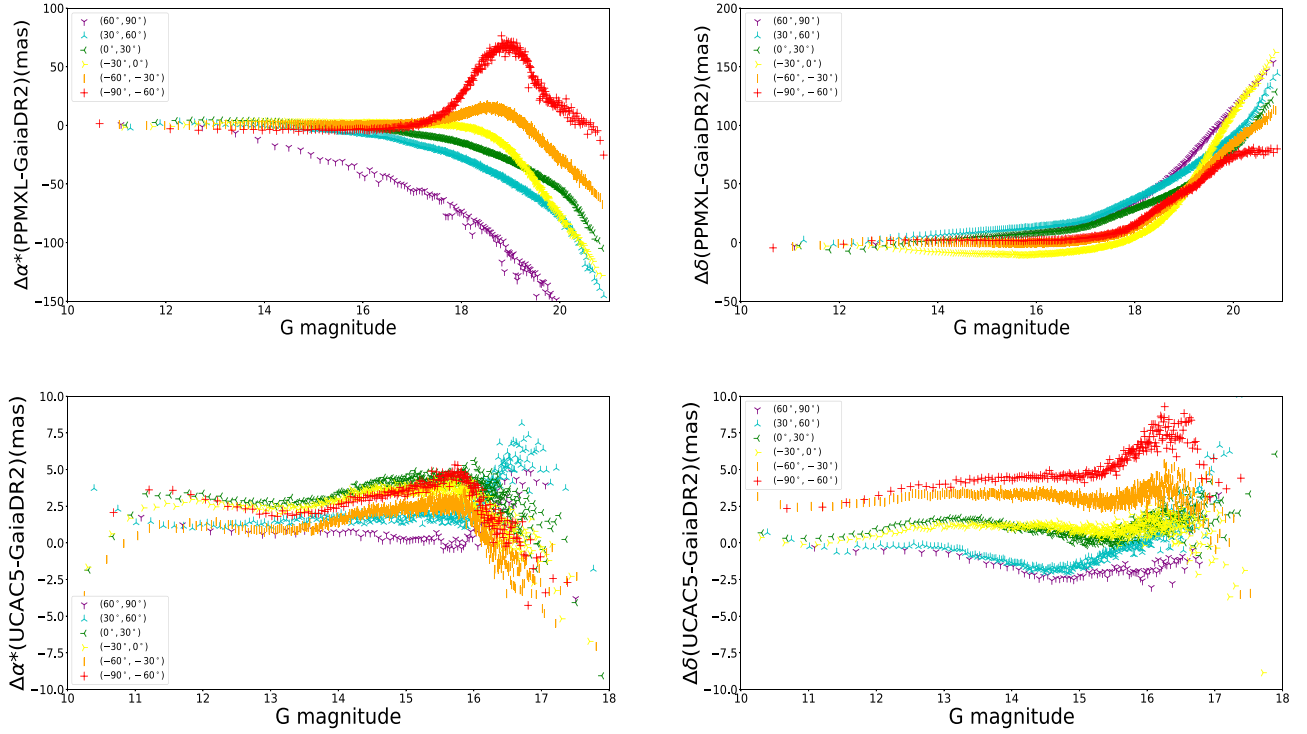
Figure 1. Mean positional differences of [PPMXL−*Gaia* DR2] and [UCAC5−*Gaia* DR2] as a function of *G* magnitude. Different color points correspond to the mean offset in different decl. zones. Scales of the different figures are different for the sake of better visual effect.
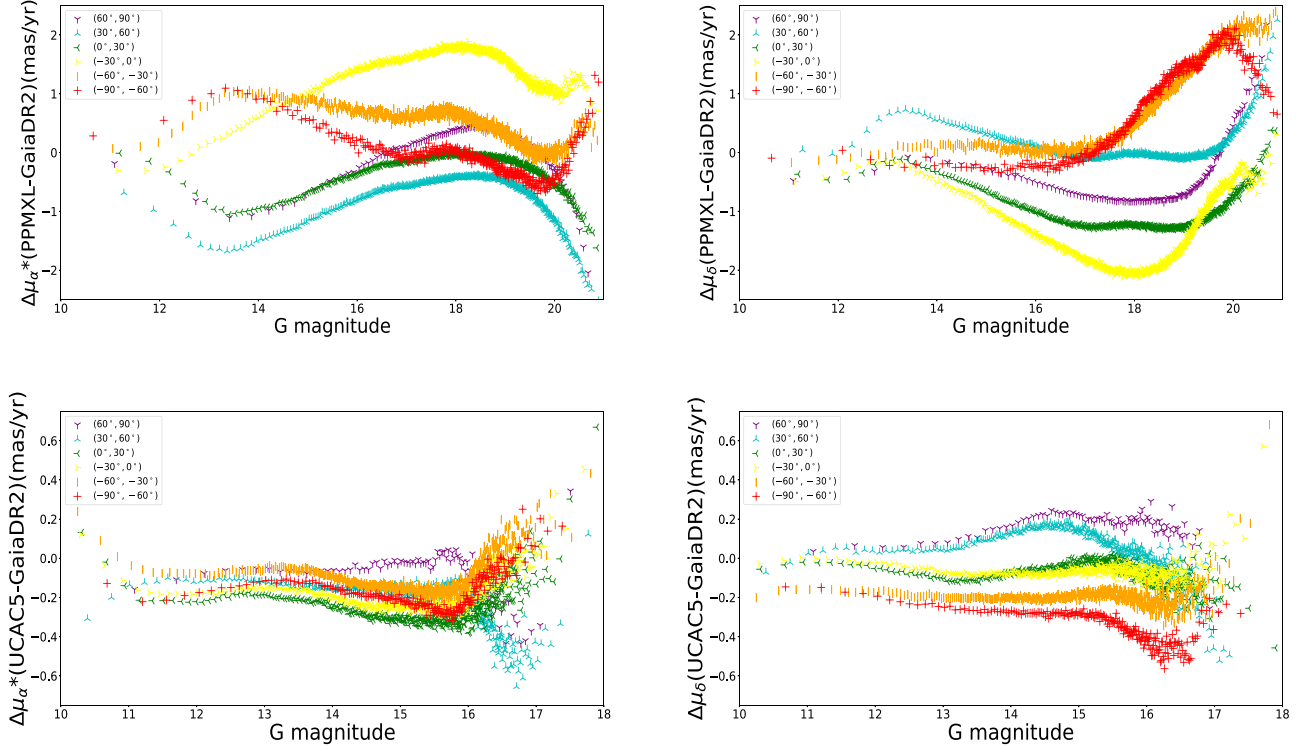

Figure 2. Mean proper-motion differences of [PPMXL−*Gaia* DR2] and [UCAC5−*Gaia* DR2] as a function of *G* magnitude. Different color points correspond to the mean offset in different decl. zones. Scales of the different figures are different for the sake of better visual effect.

3.1. Magnitude-dependent Systematic Errors

Figures 1 and 2 show magnitude-dependent differences of stellar positions and PMs in the UCAC5 and PPMXL catalogs compared with the *Gaia* DR2.

The top left panel of Figure 1 shows the dependency of the right ascension (R.A.) differences on the *G* magnitude between the PPMXL and *Gaia* DR2. We can find a bump at $G = 19$ mag in R.A. offsets for two decl. bands between $-90°$ and $-30°$, which is different from the tendency of other decl. belts. As for the
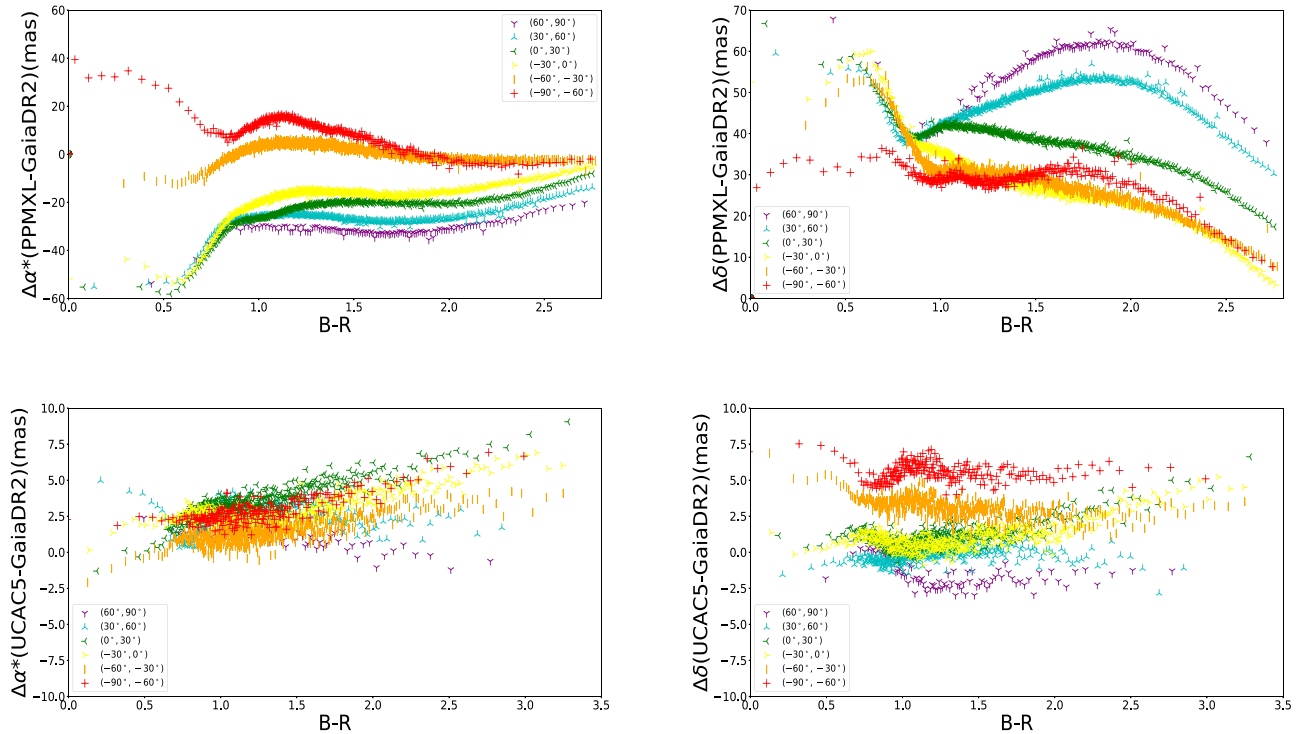
Figure 3. Mean positional differences of [PPMXL−*Gaia* DR2] and [UCAC5−*Gaia* DR2] as a function of BP–RP color. Different color points correspond to the mean offset in different decl. zones. Scales of the different figures are different for the sake of better visual effect.

decl. offsets (top right panel of Figure 1), one can see an obvious increasing trend at the faint end, and this trend holds almost the same for the whole sky. The mean PM differences between the PPMXL and *Gaia* DR2 could reach a maximum of 2.5 mas yr^{-1}. This result is reasonable because Roeser et al. (2010) stated that the absolute proper motions given in PPMXL have an underlying systematic uncertainty of at least $1 - 2$ mas yr^{-1}. Similar to the R.A. differences in Figure 1. (left-top), the PM differences in regions below $-30°$ show different behaviors from the other part in the sky.

The positional differences in the UCAC5 and *Gaia* DR2 (bottom of Figure 1) are stable when the *G* magnitude is smaller than 15 but become noisier at the fainter end. This may be due to the fact that the UCAC5 uses the TGAS stars within the range of 8 to 11 mag as reference stars (Zacharias et al. 2017). The PM differences between the UCAC5 and *Gaia* DR2 show negligible dependencies on the *G* magnitude ($G < 16$), which is similar to the positional differences as shown in the bottom panels in Figure 1. The UCAC5 PMs present larger differences with respect to the *Gaia* DR2 for faint stars due to the limiting magnitude of the reference stars in TGAS. The internals between different decl. belts are not obvious in the left-bottom panel of Figure 2. The offsets of PM in decl. are found to be positive in the northern sky but negative in the south, indicating sky-location-dependent distortions in the UCAC5 PM system. Zacharias et al. (2017) pointed out that the remaining systematic positional errors are expected not to exceed 10 mas, which corresponds to the systematics of above 0.7 mas yr^{-1} for PMs. Our results agree well with the previous conclusion.

3.2. Color-dependent Systematic Errors

For the common sources of the PPMXL and *Gaia* DR2, 98.9% of the sources have the B−R color information, and for

the UCAC5 the ratio is 99.9%. As a result, the sample of sources used in this section is slightly different from what we used in the last section (Section 3.1), but this will not affect our results of comparisons. Figures 3 and 4 show differences of stellar positions and PMs versus the color (B−R) in the UCAC5 and PPMXL catalogs compared with the *Gaia* DR2.

Between the PPMXL and *Gaia* DR2, offsets in the RA of decl. bands between $-90°$ and $-30°$ have bumps at B−R = 1.2, which is different from the other bands (top left panel of Figure 3). We found positive offsets in the decl. in PPMXL, possibly indicating a global decl. bias in the PPMXL. Besides, the tendency of decl. offsets in the southern sky is different from the northern. As for the PMs, the PM differences in R.A. yield a decl.-dependent feature: PM differences descend at first when B−R is smaller than 0.8 and ascend for decl. bands between $-90°$ and $-30°$; they increase first and tend to be stable or descend slightly at B−R > 1.2 for other bands. Similar dependency could be found in the PM differences in the decl. Our results show sky-location-dependent distortions in the PM system of the PPMXL catalog, although the authors of the PPMXL have corrected the global systematics PM system using the UCAC3 and PPMX catalogs (Roeser et al. 2010).

Things are different for the UCAC5. Positional differences between the UCAC5 and *Gaia* DR2 have no clear tendency as a function of the B−R color. But a plate structure of the underlying survey is clearly visible, which leads to a positional offset of $\sim$0.12 mas among decl. bands. The positional offset, however, is insignificant relative to formal uncertainties of positional differences ($\sim$10 mas). Similar results could be seen in the PMs system with a decl.-dependent offset of 0.1 mas yr^{-1}. In addition, the UCAC5 PM system in RA presents a negative offset with respect to the *Gaia* DR2.
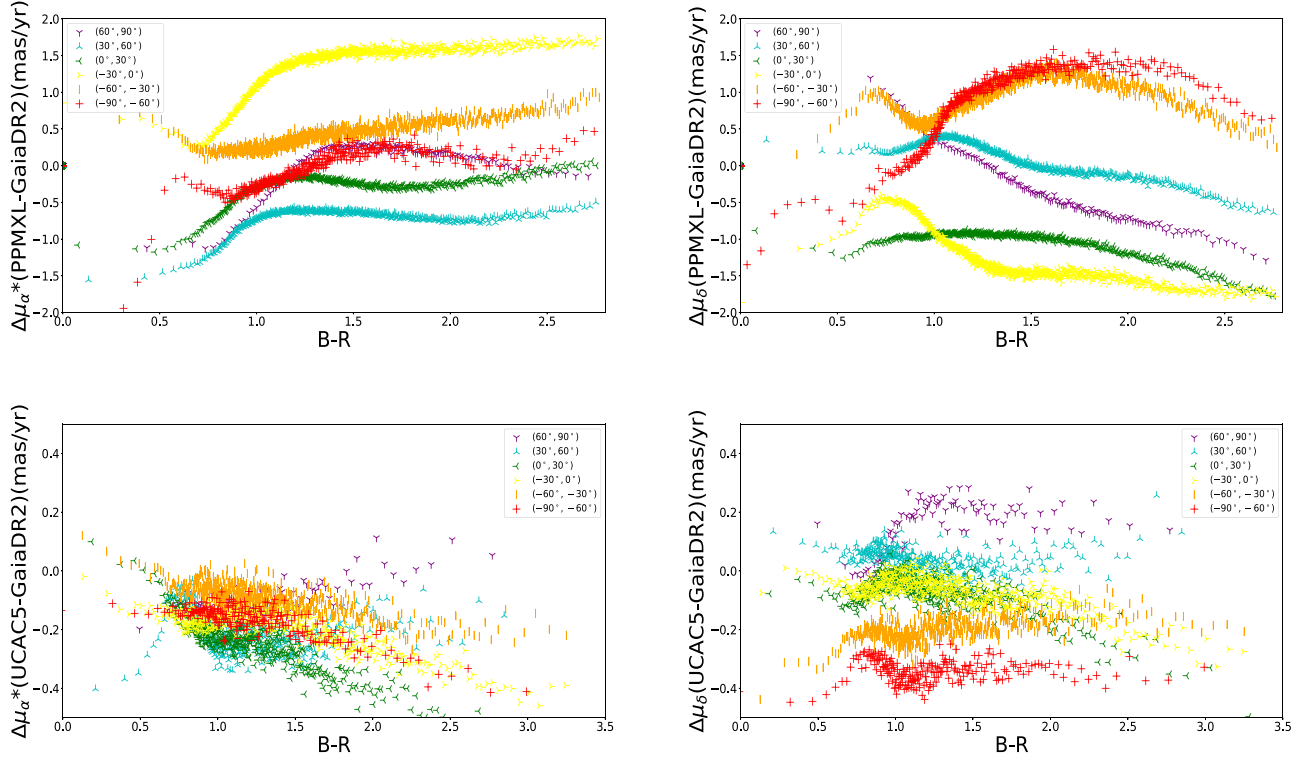
Figure 4. Mean proper-motion differences of [PPMXL−*Gaia* DR2] and [UCAC5−*Gaia* DR2] as a function of BP–RP color. Different color points correspond to the mean offset in different decl. zones. Scales of the different figures are different for the sake of better visual effect.
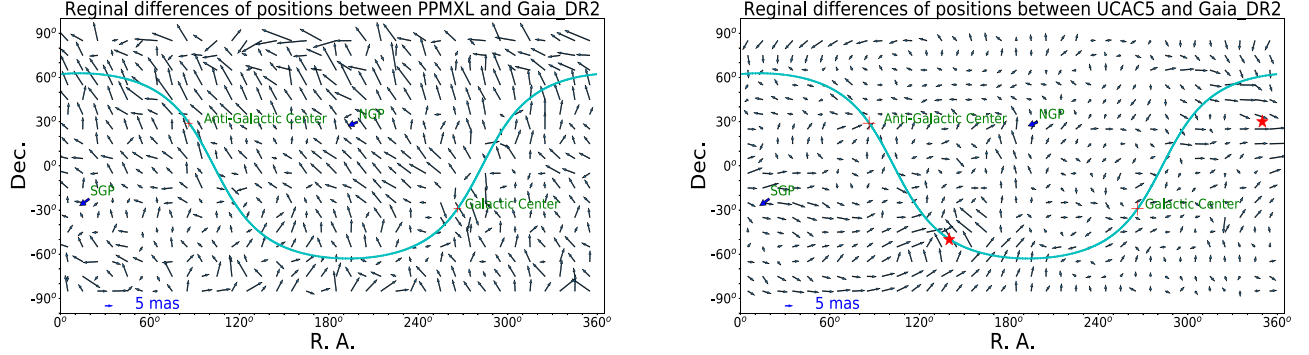

Figure 5. Mean positional differences of the PPMXL (left) and UCAC5 (right) with respect to the *Gaia* DR2, referring to a grid with $10° \times 10°$ bins. The north galactic pole, the south galactic pole, and the galactic plane are plotted in the figures. The plotting scales of the left and right panels are drew with the same scale and are given in the lower left corner of the figures.

4. Region-dependent Systematic Errors

4.1. All-sky Distribution

We divided the celestial sphere into 36×18 cells of $10° \times 10°$ in order to investigate zonal errors. In each cell, we calculated the rms of position and proper-motion differences of all entries and removed the outliers using the 3σ criterion. Then the mean differences of the positions and PMs in each cell were calculated.

All-sky distributions of the position and proper-motion differences between catalogs are displayed in Figures 5 and 6. Positional and PM differences in the regions near the south and north poles are more chaotic because of the sparsity of the sources. On average, the positional difference of the northern sky between the PPMXL and *Gaia* DR2 is 4.5 mas, larger than that of the southern. Similar features could be found in the PM differences (left of Figure 6). With respect to the *Gaia* DR2, the differences in positions and PMs in the UCAC5 are much

smaller compared with that of the PPMXL. Some local distortions, however, are more visible in the fields near $\alpha = 140°$, $\delta = -50°$, and $\alpha = 350°$, $\delta = 30°$ (indicated by red stars in the Figure 5). There is a southward tendency at $\alpha \simeq 180°$ and low declinations for positional differences.

4.2. Representation of the Systematic Errors

In this section, we applied the vector spherical harmonics (VSH) method to represent the global differences between catalogs. The principle of VSH is to use a set of orthogonal base functions (toroidal and spheroidal) to represent a vector field on a sphere (Mignard & Klioner 2012). We used the first two degrees to reveal more detailed features besides the global features. The expression of the first degree can be denoted with a rotation vector $\boldsymbol{R} = (R_1, R_2, R_3)^T$ and a glide vector $\boldsymbol{G} = (G_1, G_2, G_3)^T$ for positional differences, and $\dot{\boldsymbol{R}} = (\dot{R}_1, \dot{R}_2, \dot{R}_3)^T$ and a glide vector $\dot{\boldsymbol{G}} = (\dot{G}_1, \dot{G}_2, \dot{G}_3)^T$ for proper-motion differences. The first-degree
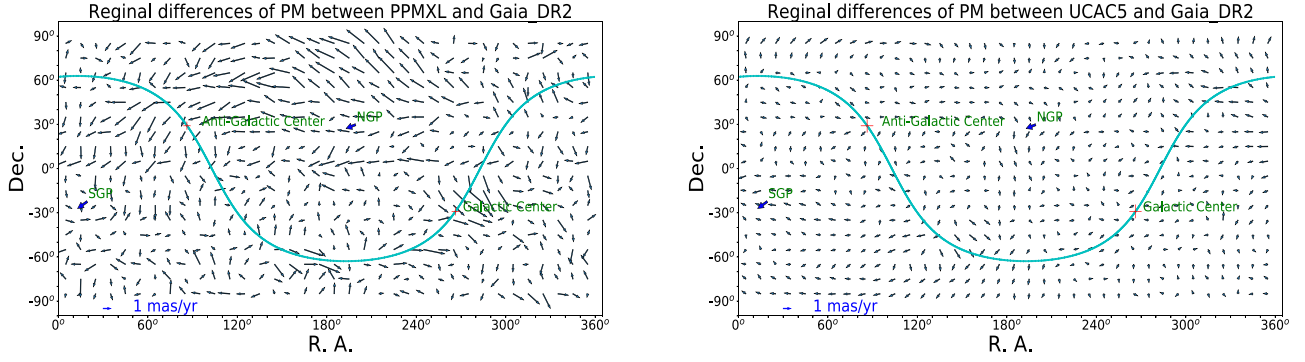
Figure 6. Mean proper-motion offsets of the PPMXL (left) and UCAC5 (right) with respect to the *Gaia* DR2. The size of each cell is $10° \times 10°$. The north galactic pole, the south galactic pole, and the galactic plane are plotted in the figures. The plotting scales of the left and right panels are drawn with the same scale and are given in the lower left corner of the figures.

description of the vector field are as follows

$$\Delta\alpha^* = +R_1 \cos\alpha \sin\delta + R_2 \sin\alpha \sin\delta$$
$$- R_3 \cos\delta - G_1 \sin\alpha + G_2 \cos\alpha,$$
$$\Delta\delta = -R_1 \sin\alpha + R_2 \cos\alpha$$
$$- G_1 \cos\alpha \sin\delta - G_2 \sin\alpha \sin\delta + G_3 \cos\delta. \quad (3)$$
$$\Delta\mu_\alpha^* = +\dot{R}_1 \cos\alpha \sin\delta + \dot{R}_2 \sin\alpha \sin\delta$$
$$- \dot{R}_3 \cos\delta - \dot{G}_1 \sin\alpha + \dot{G}_2 \cos\alpha,$$
$$\Delta\mu_\delta = -\dot{R}_1 \sin\alpha + \dot{R}_2 \cos\alpha$$
$$- \dot{G}_1 \cos\alpha \sin\delta - \dot{G}_2 \sin\alpha \sin\delta + \dot{G}_3 \cos\delta. \quad (4)$$

For the second degree, the quadrupolar vector field of the mean position and proper-motion differences can be written as follows:

$$\Delta\alpha^* = +M_{2,0} \sin 2\delta$$
$$- \cos 2\delta (M_{2,1}^{Re} \cos\alpha - M_{2,1}^{Im} \sin\alpha)$$
$$+ \sin\delta (E_{2,1}^{Re} \sin\alpha + E_{2,1}^{Im} \cos\alpha)$$
$$- \sin 2\delta (M_{2,2}^{Re} \cos 2\alpha - M_{2,2}^{Im} \sin 2\alpha)$$
$$- 2\cos\delta (E_{2,2}^{Re} \sin 2\alpha + E_{2,2}^{Im} \cos 2\alpha),$$
$$\Delta\delta = +E_{2,0} \sin 2\delta$$
$$- \sin\delta (M_{2,1}^{Re} \sin\alpha - M_{2,1}^{Im} \cos\alpha)$$
$$- \cos 2\delta (E_{2,1}^{Re} \cos\alpha + E_{2,1}^{Im} \sin\alpha)$$
$$+ 2\cos\delta (M_{2,2}^{Re} \sin 2\alpha - M_{2,2}^{Im} \cos 2\alpha)$$
$$- \sin 2\delta (E_{2,2}^{Re} \cos 2\alpha + E_{2,2}^{Im} \sin 2\alpha). \quad (5)$$

$$\Delta\mu_\alpha^* = +\dot{M}_{2,0} \sin 2\delta$$
$$- \cos 2\delta (\dot{M}_{2,1}^{Re} \cos\alpha - \dot{M}_{2,1}^{Im} \sin\alpha)$$
$$+ \sin\delta (\dot{E}_{2,1}^{Re} \sin\alpha + \dot{E}_{2,1}^{Im} \cos\alpha)$$
$$- \sin 2\delta (\dot{M}_{2,2}^{Re} \cos 2\alpha - \dot{M}_{2,2}^{Im} \sin 2\alpha)$$
$$- 2\cos\delta (\dot{E}_{2,2}^{Re} \sin 2\alpha + \dot{E}_{2,2}^{Im} \cos 2\alpha)$$
$$\Delta\mu_\delta = +\dot{E}_{2,0} \sin 2\delta$$
$$- \sin\delta (\dot{M}_{2,1}^{Re} \sin\alpha - \dot{M}_{2,1}^{Im} \cos\alpha)$$
$$- \cos 2\delta (\dot{E}_{2,1}^{Re} \cos\alpha + \dot{E}_{2,1}^{Im} \sin\alpha)$$
$$+ 2\cos\delta (\dot{M}_{2,2}^{Re} \sin 2\alpha - \dot{M}_{2,2}^{Im} \cos 2\alpha)$$
$$- \sin 2\delta (\dot{E}_{2,2}^{Re} \cos 2\alpha + \dot{E}_{2,2}^{Im} \sin 2\alpha). \quad (6)$$

The orthogonality conditions between the different base functions are preserved only if the distribution of the sources on the unit sphere is uniform (Mignard & Klioner 2012). The solved parameters will be weakly correlated and more robust when the orthogonality conditions are preserved. Actually, plenty of sources assemble near galactic center while the stars are sparse near galactic poles. To ensure the orthogonality of the function set, we project the R.A. and decl. (α, δ) to $(a = \alpha, b = \cos\delta)$. Then we divided the a and b into 360×180 cells uniformly and calculated the mean differences of the positions and PMs in each cell.

The obtained VSH parameters for position and proper-motion differences are given in Figures 7 and 8, respectively. The value of VSH parameters are shown in Tables 1 and 2 in Appendix A. We found a significant glide component $G_3 \sim 8$ mas and rotation component $R_3 \sim -5$ mas with respect to their formal error in positional offsets between PPMXL and *Gaia* DR2. As for the second-degree parameters, $E_{2,2}^{Re}$, $E_{2,0}$, and $M_{2,0}$ are found to exceed 1 mas. Since G_3 and $E_{2,0}$ only appear in the expression of $\Delta\delta$ (Equation (3)), they can partly explain the large upward trend in Figure 5 (left). Similarly, the large leftward trend in Figure 5 (left), corresponding mostly to $\Delta\alpha$, could also be explained by the R_3 term. For the PMs of the PPMXL, the first-degree parameters are almost at the same level of 0.65 mas yr^{-1}. One quadrupolar term $\dot{M}_{2,0}$ is estimated to be about 1 mas yr^{-1} while other terms are on the level of 0.1 mas yr^{-1}. For the positions of UCAC5, two orientation terms of R_2 and R_3 on the level of ~ 2 mas are found with respect to the *Gaia* DR2 positions. These two terms are consistent with the features (rotations and rightward vectors) found in Figure 5. Three quadrupolar terms are reported to be larger than 1 mas, which is consisted of $E_{2,1}^{Re}$, $M_{2,1}^{Re}$, and $M_{2,0}^{Re}$. The PM system of the UCAC5 yields first-degree parameters at the same level of 0.1 mas yr^{-1}, 5 times smaller than that of the PPMXL. No significant quadrupolar parameters (greater than 0.1 mas yr^{-1}) are found.

The correlation coefficients of the first degree in solutions are given in Tables 3–4 in Appendix A. For the second degree, the correlation coefficients are not given in the paper because there is no significant coefficient (larger than 0.5). There are two significant correlation coefficients in the solution of the proper-motion differences of the first degree between the PPMXL and *Gaia* DR2. For example, the correlation coefficient between $\dot{R}_2$ and $\dot{G}_1$ is larger than 0.5. From Equation (4), we can find that $\dot{R}_2$ and $\dot{G}_1$
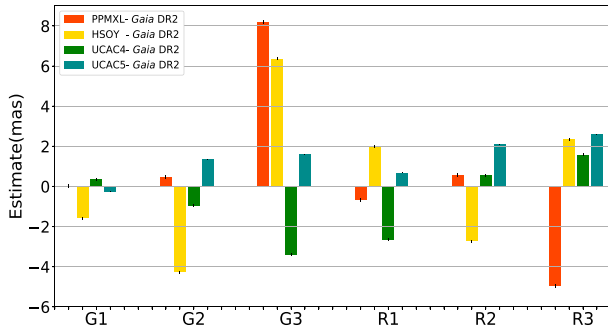
6

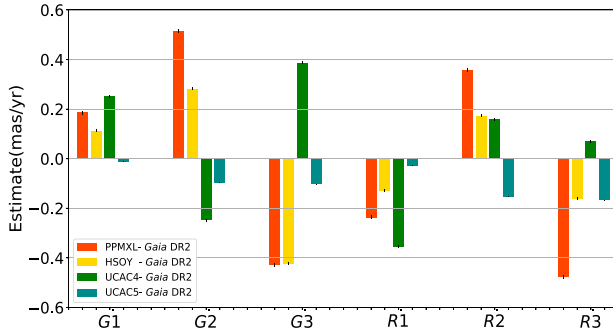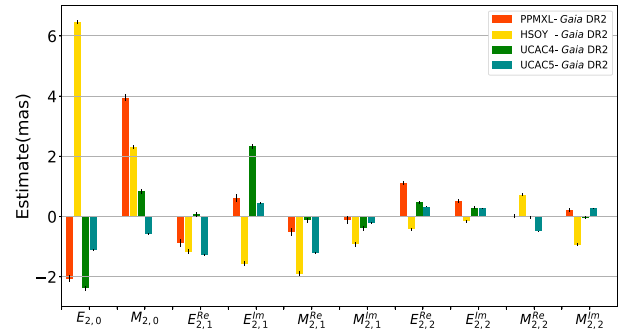**Figure 7.** VSH parameters of positional differences.

Figure 8. VSH parameters of proper-motion differences.

have the same coefficient ($\sin\delta$). This argument holds similar between $\dot{G}_2$ and $\dot{R}_1$.

5. Additional Comparisons

For the above different systematic errors in PPMXL and UCAC5, one cause is the different observation methods of the catalogs. The PPMXL is based on the scans of Schmidt plates while UCAC5 is based on CCD observations. Another possible reason is that the UCAC5 has used the TGAS in the *Gaia* DR1 as its reference catalog. To assess the influence of the reference catalogs, we perform similar analyses to the UCAC4 and HSOY. UCAC4 uses the Tycho-2 as a reference catalog and almost shares the same observation data with the UCAC5 (Zacharias et al. 2013) and HSOY is the combination of PPMXL and *Gaia* DR1 (Altmann et al. 2017).

We obtained 106,617,493 common objects between UCAC4 and *Gaia* DR2, using the cross-match list of Marrese et al. (2019).[3] For UCAC4 and *Gaia* DR2, mean positional and proper-motion difference are displayed in Figures 9 and 10, and all-sky distributions of the differences are shown in Figure 13 in the Appendix B. The trends of R.A. differences for the decl. belts between $-90°$ and $-30°$ are very different from that of other decl. belts (top left panels of Figures 9 and 10). This is different from that of UCAC5. Another difference with the UCAC5 is that the proper-motion differences between UCAC4 and *Gaia* DR2 show obvious dependencies on the G magnitude and B−R. Moreover, the norms of the vectors of positional and proper-motion difference between UCAC4 and *Gaia* DR2 are generally larger than that of UCAC5 and *Gaia* DR2 (Figure 13). As for the positional difference, we found a significant glide component $G_3 \sim -3$ mas and rotation

component $R_1 \sim -3$ mas. The first degree of VSH parameters for the PM system between UCAC4 and *Gaia* DR2 are almost at the same level of 0.3 mas yr^{-1}. These results show great improvement in UCAC5 from UCAC4 and confirm that the systematic errors of UCAC observations are indeed partly calibrated by *Gaia* data.

As for HSOY and *Gaia* DR2, we obtained 556,596,424 common objects by using the link between the *Gaia* DR1 and DR2 entries. The positional and proper-motion differences between HSOY and *Gaia* DR2 are given in Figures 11 and 12 and all-sky distributions of the differences are displayed in Figure 14. The positional differences present opposite trends versus G magnitude and B−R to that of the proper-motion differences (Figures 11 and 12). This indicates that the positions and proper motions of HSOY probably have correlations. In addition, comparing the top panels of Figure 1 with the top panels of Figure 11, we found that the dependency of positional differences on G magnitude between the HSOY and *Gaia* DR2 is similar to that of the PPMXL and *Gaia* DR2. The dependency of positional differences on B−R also has a similar tendency (top panels of Figure 3 and top panels of Figure 12). It shows that the position system of HSOY is likely to inherit the systematic errors of PPMXL. As for the all-sky distributions, the vectors of positional differences between HSOY and *Gaia* DR2 are comparable to that between PPMXL and *Gaia* DR2 (left panel of Figure 5 and left panel of Figure 14). The PM differences between HSOY and *Gaia* DR2 are smaller than that between PPMXL and *Gaia* DR2 (left panel of Figure 6 and right panel of Figure 14). Furthermore, the first-degree parameters of the PM differences are on the level of 0.2 mas yr^{-1}, which is smaller than that of PPMXL. In general, the PM systematic differences of HSOY are smaller than that of PPMXL.

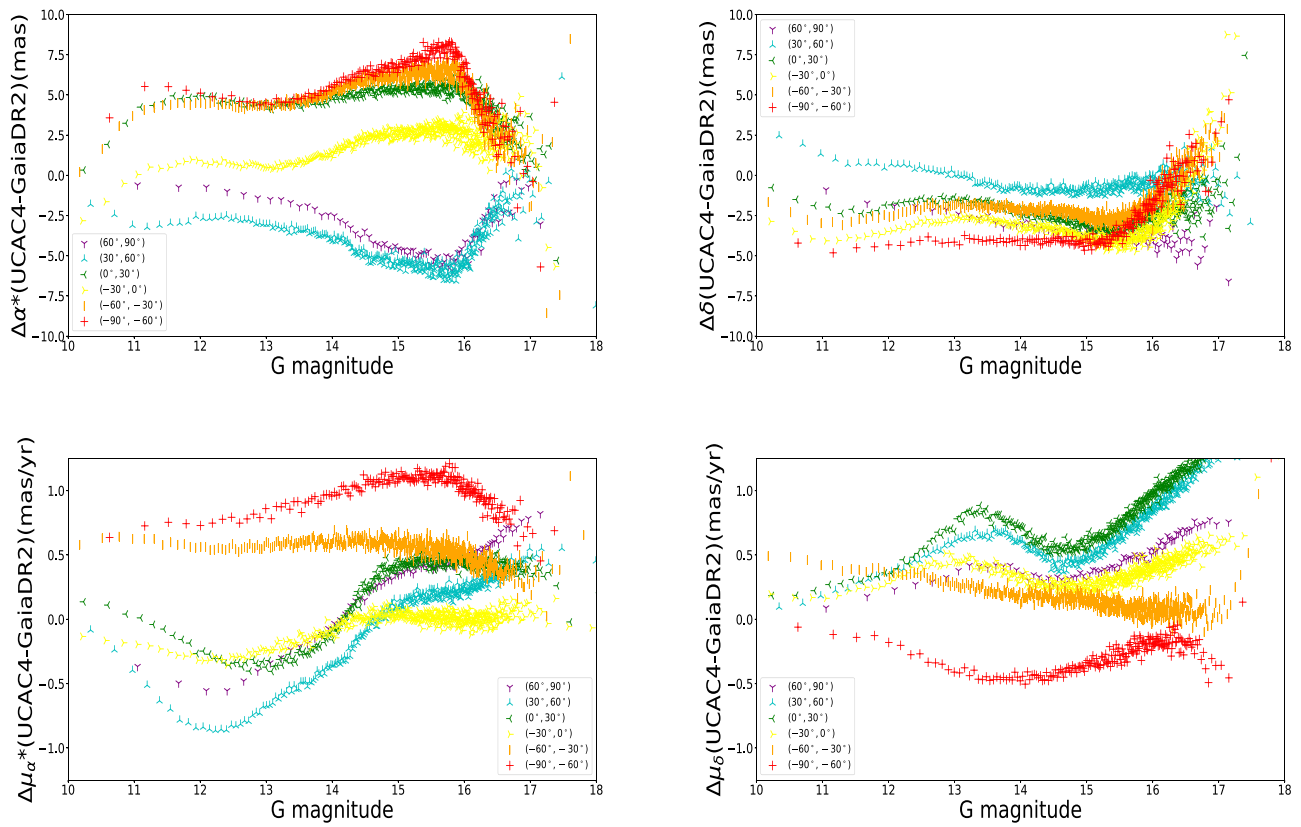[3] The list could be found in http://gea.esac.esa.int/archive/.

Figure 9. Mean positional and proper-motion differences of [UCAC4−*Gaia* DR2] as a function of *G* magnitude. Different color points correspond to the mean offset in different decl. zones.

Figure 10. Mean positional and proper-motion differences of [UCAC4−*Gaia* DR2] as a function of BP–RP color. Different color points correspond to the mean offset in different decl. zones.

Figure 11. Mean positional and proper-motion differences of [HSOY−*Gaia* DR2] as a function of *G* magnitude. Different color points correspond to the mean offset in different decl. zones.
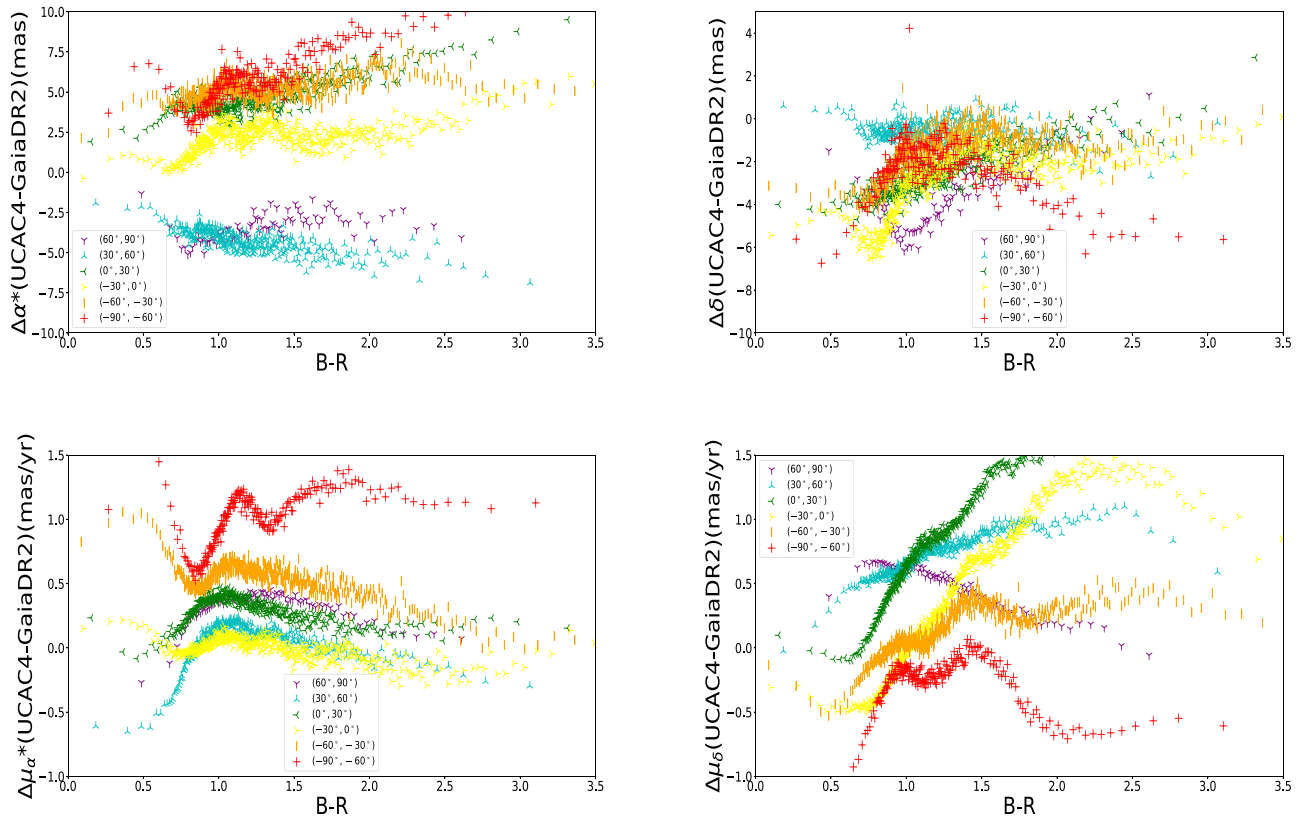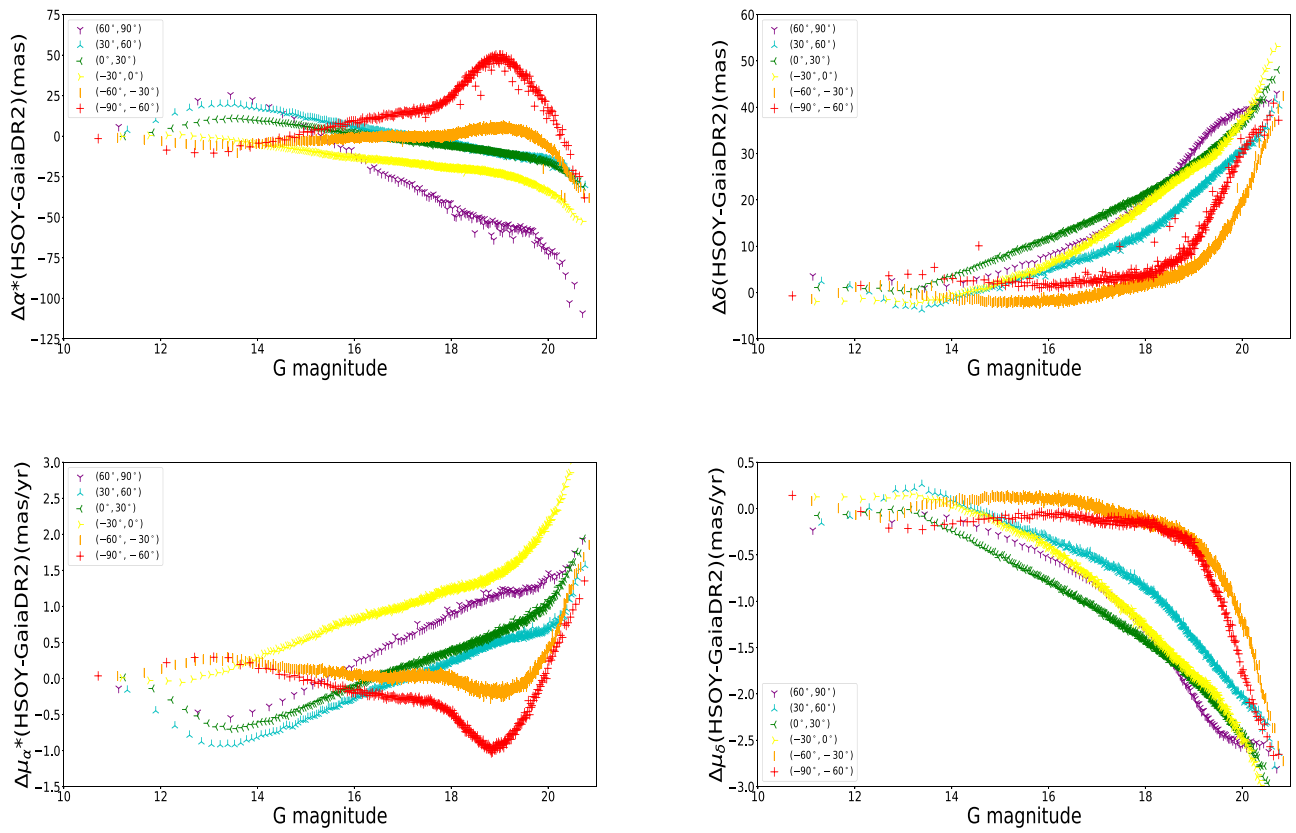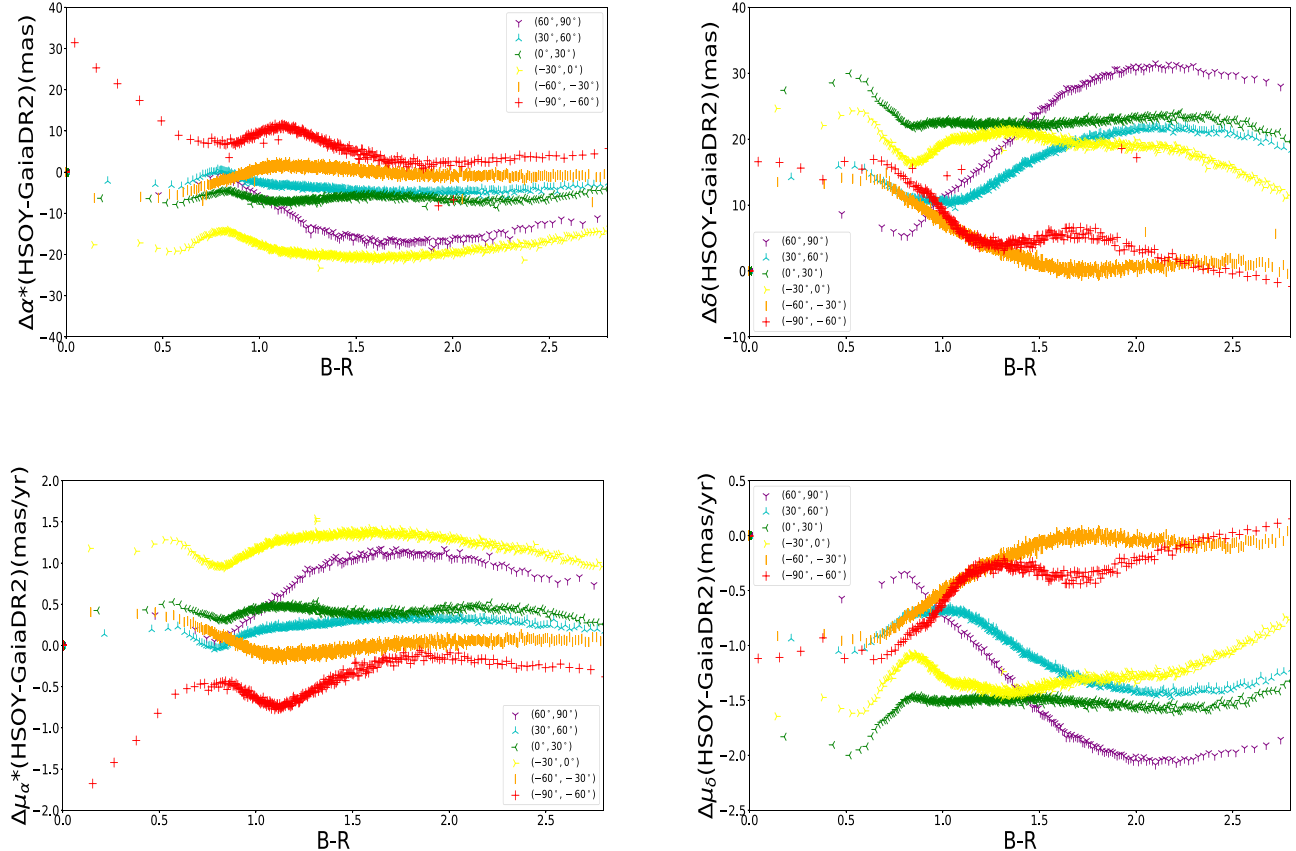

Figure 12. Mean positional and proper-motion differences of [HSOY−*Gaia* DR2] as a function of BP–RP color. Different color points correspond to the mean offset in different decl. zones.

6. Concluding Remarks

We have shown magnitude-, color-, and sky-location-dependent systematic errors in the position and proper-motion systems of the PPMXL and UCAC5 compared with the *Gaia* DR2, especially at the faint end (*G* magnitude is larger than 15). These systematic errors between the PPMXL and *Gaia* DR2 are found to be larger than those between the UCAC5 and *Gaia* DR2. The fitted VSH parameters reflected misorientation and distortions in the global- and local-scales in the PPMXL and UCAC5, if we assume that the position and proper-motion system of the *Gaia* DR2 are perfect. Orientation offset, dipolar deformations, and quadrupolar deformations up to several mas are reported in the positions of both catalogs. There are also significant VSH terms on the level of $0.1\,\mathrm{mas\,yr^{-1}}$ in the proper-motion systems of the PPMXL and UCAC5.

Even though catalogs used in this paper are on the ICRS systems, they were built in different ways. PPMXL inherits the system from its predecessor PPMX and is partly calibrated by the UCAC3 catalog for regions with $\delta < -20°$. The UCAC5 is on the ICRS system represented by the *Gaia*-CRF1 or, more specifically, the TGAS. The *Gaia* DR2 is on its own reference frame, which is called the *Gaia*-CRF2. The VSH parameters of several mas in positions and of $0.1\,\mathrm{mas\,yr^{-1}}$ in proper motions cannot be fully attributed to differences between reference frames. In general, the reconstruction of UCAC5 is excellent,

removing many systematic errors in observation data. Though some systematic errors of PPMXL are inherited in HSOY, the PM system of HSOY is generally better than that of PPMXL. Our results confirm the benefits of the strategy of the space-calibrated ground-based catalog.

Appendix A
VSH Parameters

The VSH parameters for positional and proper-motion differences are shown in Tables 1 and 2. Tables 3–4 are the correlation coefficients in solutions.

Table 1
VSH Parameters (mas) for Positional Difference

	PPMXL - *Gaia* DR2		UCAC5 - *Gaia* DR2	
Glide				
G_1	0.044 ± 0.099		-0.274 ± 0.021	
G_2	0.451 ± 0.097		1.364 ± 0.021	
G_3	8.176 ± 0.094		1.609 ± 0.020	
Amplitude	8.189 ± 0.094		2.091 ± 0.021	
Rotation				
R_1	-0.692 ± 0.099		0.680 ± 0.021	
R_2	0.581 ± 0.097		2.111 ± 0.020	
R_3	-4.962 ± 0.095		2.603 ± 0.021	
Amplitude	5.044 ± 0.095		3.420 ± 0.021	
Quadrupole	Re	Im	Re	Im
$E_{2,0}$	3.950 ± 0.108		-0.580 ± 0.023	
$E_{2,1}$	-0.883 ± 0.120	0.610 ± 0.122	-1.268 ± 0.026	0.453 ± 0.027
$E_{2,2}$	1.104 ± 0.060	0.501 ± 0.060	0.332 ± 0.013	0.271 ± 0.013
$M_{2,0}$	-2.075 ± 0.108		-1.098 ± 0.023	
$M_{2,1}$	-0.529 ± 0.121	-0.121 ± 0.122	-1.213 ± 0.027	-0.231 ± 0.027
$M_{2,2}$	0.010 ± 0.059	0.214 ± 0.060	-0.481 ± 0.013	0.269 ± 0.013
Amplitude	4.766 ± 0.107		2.521 ± 0.023	

Table 2
VSH Parameters (mas yr^{-1}) for Proper-motion Difference

	PPMXL - *Gaia* DR2		UCAC5 - *Gaia* DR2	
Glide				
$\dot{G}_1$	0.186 ± 0.008		-0.013 ± 0.002	
$\dot{G}_2$	0.514 ± 0.008		-0.096 ± 0.002	
$\dot{G}_3$	-0.429 ± 0.007		-0.103 ± 0.002	
Amplitude	0.695 ± 0.008		0.141 ± 0.002	
Rotation				
$\dot{R}_1$	-0.237 ± 0.008		-0.029 ± 0.002	
$\dot{R}_2$	-0.359 ± 0.008		-0.154 ± 0.002	
$\dot{R}_3$	-0.478 ± 0.007		-0.167 ± 0.002	
Amplitude	0.643 ± 0.007		0.229 ± 0.002	
Quadrupole	Re	Im	Re	Im
$\dot{E}_{2,0}$	0.027 ± 0.008		0.032 ± 0.002	
$\dot{E}_{2,1}$	0.076 ± 0.009	0.187 ± 0.009	0.088 ± 0.002	-0.024 ± 0.002
$\dot{E}_{2,2}$	0.122 ± 0.004	0.073 ± 0.005	-0.014 ± 0.001	-0.017 ± 0.001
$\dot{M}_{2,0}$	-0.953 ± 0.008		0.045 ± 0.002	
$\dot{M}_{2,1}$	0.219 ± 0.009	0.053 ± 0.009	0.081 ± 0.002	0.000 ± 0.002
$\dot{M}_{2,2}$	-0.099 ± 0.004	0.129 ± 0.005	0.037 ± 0.001	-0.014 ± 0.001
Amplitude	1.430 ± 0.006		0.329 ± 0.002	

Table 3
Correlation Coefficients of Parameters in the First Degree of VSH for the UCAC5 and *Gaia* DR2

	G_2	G_3	R_1	R_2	R_3		$\dot{G}_2$	$\dot{G}_3$	$\dot{R}_1$	$\dot{R}_2$	$\dot{R}_3$
G_1	$+0.0$	-0.0	$+0.0$	-0.0	$+0.1$	$\dot{G}_1$	$+0.0$	-0.0	$+0.0$	$+0.2$	$+0.1$
G_2		-0.0	$+0.0$	-0.0	$+0.0$	$\dot{G}_2$		-0.0	-0.2	-0.0	$+0.0$
G_3			-0.1	$+0.0$	-0.0	$\dot{G}_3$			-0.1	-0.0	-0.0
R_1				$+0.0$	-0.0	$\dot{R}_1$				$+0.0$	-0.0
R_2					-0.0	$\dot{R}_2$					-0.0

Table 4
Correlation Coefficients of Parameters in the First Degree of VSH for the PPMXL and *Gaia* DR2

	G_2	G_3	R_1	R_2	R_3		$\dot{G}_2$	$\dot{G}_3$	$\dot{R}_1$	$\dot{R}_2$	$\dot{R}_3$
G_1	$+0.0$	-0.0	$+0.0$	-0.3	$+0.1$	$\dot{G}_1$	-0.0	-0.0	$+0.0$	-0.5	$+0.1$
G_2		-0.0	$+0.3$	-0.0	-0.0	$\dot{G}_2$		-0.0	$+0.5$	-0.0	-0.1
G_3			-0.1	$+0.0$	-0.0	$\dot{G}_3$			-0.1	$+0.1$	$+0.0$
R_1				$+0.0$	-0.0	$\dot{R}_1$				-0.0	-0.0
R_2					-0.0	$\dot{R}_2$					-0.0

Appendix B
Additional Comparisons of [UCAC4−*Gaia* DR2] and [HSOY−*Gaia* DR2]

Figures 9–12 present the mean positional and proper-motion differences of [UCAC4−*Gaia* DR2] and [HSOY−*Gaia* DR2] as a function of G magnitude or B−R color. The all-sky distributions of position and proper-motion differences of [UCAC4−*Gaia* DR2] and [HSOY−*Gaia* DR2] are displayed in Figures 13 and 14.
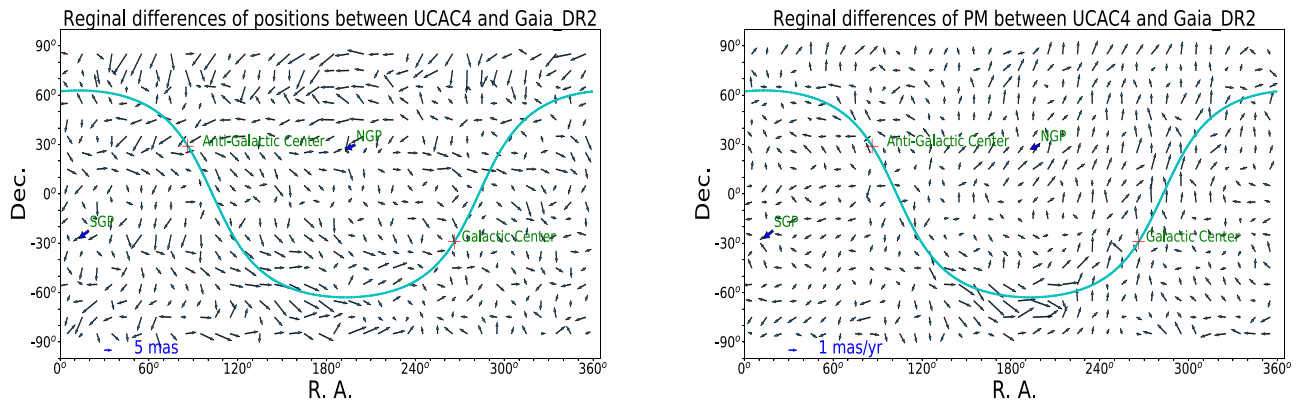
Figure 13. Mean positional and proper-motion offsets of the UCAC4 with respect to the *Gaia* DR2. The size of each cell is 10° × 10°. The north galactic pole, the south galactic pole, and the galactic plane are plotted in the figures. The plotting scales are given in the lower left corner of each panel.
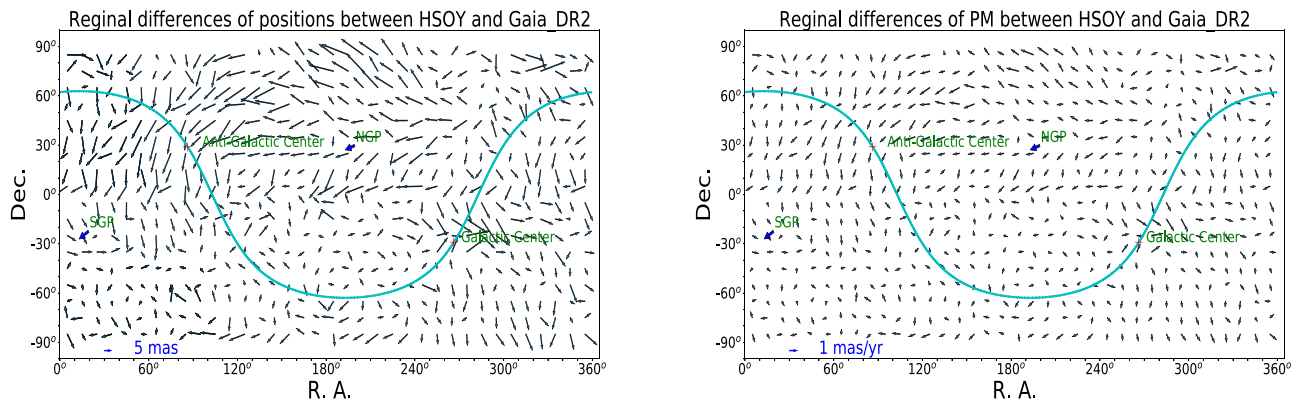

Figure 14. Mean positional and proper-motion differences of HSOY with respect to the *Gaia* DR2, referring to a grid with 10° × 10° bins. The north galactic pole, the south galactic pole, and the galactic plane are plotted in the figures. The plotting scales are given in the lower left corner of each panel.

ORCID iDs

Z. Zhu ⓘ https://orcid.org/0000-0001-6868-0231
J.-C. Liu ⓘ https://orcid.org/0000-0002-6637-9258

References

Altmann, M., Roeser, S., Demleitner, M., et al. 2017, A&A, 600, L4
ESA 1997, in ESA Special Publication 1200, The HIPPARCOS and TYCHO Catalogues: Astrometric and Photometric Star Catalogues Derived from the ESA HIPPARCOS Space Astrometry Mission (Noordwijk: ESA), ESA SP-1200
Fricke, W., Schwan, H., Lederle, T., et al. 1988, VeARI, 32, 1
Gaia Collaboration, Brown, A. G. A., Vallenari, A., et al. 2016b, A&A, 595, A2
Gaia Collaboration, Brown, A. G. A., Vallenari, A., et al. 2018, A&A, 616, A1
Gaia Collaboration, Prusti, T., de Bruijne, J. H. J., et al. 2016a, A&A, 595, A1
Høg, E., Fabricius, C., Makarov, V. V., et al. 2000, A&A, 355, L27
Lindegren, L., Hernández, J., Bombrun, A., et al. 2018, A&A, 616, A2
Lindegren, L., Lammers, U., Bastian, U., et al. 2016, A&A, 595, A4
Liu, J.-C., Zhu, Z., & Hu, B. 2011, RAA, 11, 1074

Ma, C., Arias, E. F., Eubanks, T. M., et al. 1998, AJ, 116, 516
Marrese, P. M., Marinoni, S., Fabrizio, M., et al. 2019, A&A, 621, A144
Mignard, F., & Frœschlé, M. 2000, A&A, 354, 732
Mignard, F., & Klioner, S. 2012, A&A, 547, A59
Monet, D. G., Levine, S. E., Canzian, B., et al. 2003, AJ, 125, 984
Perryman, M. A. C., Lindegren, L., Kovalevsky, J., et al. 1997, A&A, 323, L49
Riello, M., De Angeli, F., Evans, D. W., et al. 2018, A&A, 616, A3
Roeser, S., Demleitner, M., & Schilbach, E. 2010, AJ, 139, 2440
Röser, S., & Bastian, U. 1993, BICDS, 42, 11
Röser, S., Schilbach, E., Schwan, H., et al. 2008, A&A, 488, 401
Skrutskie, M. F., Cutri, R. M., Stiening, R., et al. 2006, AJ, 131, 1163
Taylor, M. B. 2006, in ASP Conf. Ser. 351, Astronomical Data Analysis Software and Systems XV, ed. C. Gabriel et al. (San Francisco, CA: ASP), 666
Vityazev, V. V., & Tsvetkov, A. S. 2014, MNRAS, 442, 1249
Vityazev, V. V., & Tsvetkov, A. S. 2015, AstL, 41, 317
Vityazev, V. V., & Tsvetkov, A. S. 2016, MNRAS, 461, 2410
Vityazev, V. V., Tsvetkov, A. S., Petrov, S. D., et al. 2017, AN, 338, 489
Zacharias, N., Finch, C., & Frouard, J. 2017, AJ, 153, 166
Zacharias, N., Finch, C. T., Girard, T. M., et al. 2013, AJ, 145, 44
Zhu, Z. 2000, PASP, 112, 1103